

Contact-Aware Safety in Soft Robots Using High-Order Control Barrier and Lyapunov Functions

Kiwan Wong^{1,2}, Maximilian Stölzle^{1,2,3}, Wei Xiao², Cosimo Della Santina³, Daniela Rus^{*,2}, Gioele Zardini^{*,1}

Abstract—Robots operating alongside people, particularly in sensitive scenarios such as aiding the elderly with daily tasks or collaborating with workers in manufacturing, must guarantee safety and cultivate user trust. Continuum soft manipulators promise safety through material compliance, but as designs evolve for greater precision, payload capacity, and speed, and increasingly incorporate rigid elements, their injury risk resurfaces. In this letter, we introduce a comprehensive High-Order Control Barrier Function (HOCBF) + High-Order Control Lyapunov Function (HOCCLF) framework that enforces strict contact force limits across the entire soft-robot body during environmental interactions. Our approach combines a differentiable Piecewise Cosserat-Segment (PCS) dynamics model with a convex-polygon distance approximation metric, named Differentiable Conservative Separating Axis Theorem (DCSAT), based on the soft robot geometry to enable real-time, whole-body collision detection, resolution, and enforcement of the safety constraints. By embedding HOCBFs into our optimization routine, we guarantee safety and actively regulate environmental coupling, allowing, for instance, safe object manipulation under HOCCLF-driven motion objectives. Extensive planar simulations demonstrate that our method maintains safety-bounded contacts while achieving precise shape and task-space regulation. This work thus lays a foundation for the deployment of soft robots in human-centric environments with provable safety and performance.

I. INTRODUCTION

Deploying robots in human-centered environments, such as assisting workers in manufacturing or supporting older adults in everyday activities [1], demands not only demonstrable safety but also user confidence in the robot’s behavior. Traditional rigid collaborative manipulators address this need through increasingly sophisticated algorithms for collision detection [2], [3], impedance control [4], Model Predictive Control (MPC) [5], and, more recently, Control Barrier Functions (CBFs) [6], [7]. Yet, perception errors or model inaccuracies can still expose users to hazardous impacts.

Continuum soft manipulators offer a fundamentally different path to safety: instead of relying solely on software, they seek to embed safety directly through compliance [8]. However, material softness is not a panacea [9], [10]. As the field advances toward greater precision and functionality, emerging designs are expected to incorporate increased stiffness [11], exert larger forces and velocities [12], and adopt hybrid rigid-soft architectures [13], [14]. Such developments reintroduce risks traditionally associated with rigid systems.

*D. Rus and G. Zardini contributed equally as joint senior authors.

¹Laboratory for Information and Decision Systems, Massachusetts Institute of Technology, Cambridge, MA 02139, USA {kiwan588, mstolzle, gzardini}@mit.edu. ²Computer Science and Artificial Intelligence Laboratory, Massachusetts Institute of Technology, Cambridge, MA 02139, USA {weixy, rus}@mit.edu. ³Cognitive Robotics, Delft University of Technology, Delft, 2628 CD, Netherlands {M.W.Stolzle, C.DellaSantina}@tudelft.nl.

The work by K. Wong was supported by The Hong Kong Jockey Club Scholarships; The work by M. Stölzle was supported under the European Union’s Horizon Europe Program from Project EMERGE - Grant Agreement No. 101070918, and by the Cultuurfonds Wetenschapsbeurzen 2024 and the Rudge (1948) and Nancy Allen Chair for his research visit to LIDS/Zardini Lab at MIT.

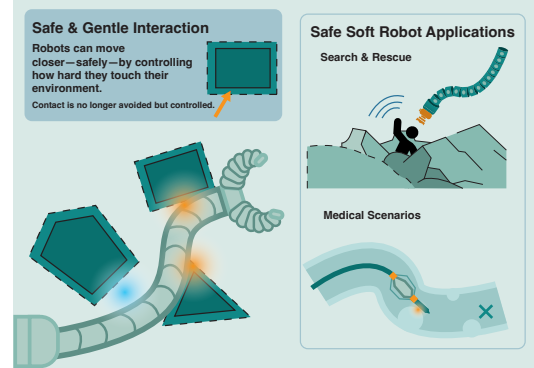


Fig. 1: **Contact Safety-Aware Control of Soft Robots with High-Order CBFs (HOCBFs) and High-Order CLFs (HOCCLFs).** Illustration of compliant contact control with safety bounds guaranteed by High-Order CBFs (HOCBFs). By respecting contact force limits, the robot can intentionally engage with its surroundings without sacrificing safety. Task goals are shaped through High-Order CLFs (HOCCLFs), while constraint satisfaction is upheld by High-Order CBFs (HOCBFs). This approach enables the secure use of soft robots in demanding settings—from search-and-rescue missions to delicate medical procedures.

Thus, mechanical compliance must be augmented with algorithmic guarantees that ensure real-time safety and foster user trust.

Our approach embraces, rather than avoids, physical contact¹, deviating from the predominant paradigm in rigid robotics [2], [15]. Instead of treating contact as a failure, we exploit the soft robot’s embodied intelligence [16]—its intrinsic physical coupling with the environment—to enhance robustness, stabilize deformation and motion, and adapt to external constraints, all while ensuring that every interaction respects safety standards such as the injury severity thresholds set out in ISO/TS 15066:2016 [15].

To date, no method explicitly enforces upper bounds on the contact force or pressure applied across the surface of a soft robot. Classical impedance and force control schemes cannot impose strict bounds [17], and recent CBF-based methods [14] address only self-contact avoidance. A newer preprint [10] adapts CBFs to constrain end-effector forces, but it neglects distributed body interactions and relies on rigid-body dynamics approximating Piecewise Constant Curvature (PCC) models [17].

We present an integrated control framework that imposes contact-force limits along the entire body of a soft manipulator. Building on the well-established CBF+Control Lyapunov Function (CLF) framework [6]—specifically its high-order extension [18]—our method keeps the system’s trajectory inside a certified safe set by solving constrained optimizations in real time. The proposed High-Order CBF (HOCBF)+High-Order CLF (HOCCLF) control scheme rests on two pillars: (i) a fully differentiable implementation of the Piecewise Constant Strain (PCS) [19], [20], and (ii) a

¹Please note that we use “contact” and “collision” interchangeably in this letter.

fast, differentiable collision-detection routine that represents the soft manipulator with convex-polygon approximations.

In support pillar (ii), we propose a new convex-polygon distance measure—Differentiable Conservative SAT (DC-SAT)—that serves as a conservative, differentiable proxy for the standard Separating Axis Theorem (SAT) metric. Compared with recent differentiable SAT surrogates such as Smooth SAT (SSAT) [21], our approach (1) systematically underestimates the separation distance, yielding the conservative buffer required for formal safety guarantees, and (2) achieves an increase of roughly 1.5–3× in computational efficiency enabling real-time, full-body collision checks. We then validate the proposed framework through extensive simulations in a planar setting.

In summary, this letter (i) develops a principled HOCBF-based method to enforce global contact force constraints on soft robots, (ii) adapts the HOCBF+HOCLF framework for shape control and task-space regulation supporting navigation tasks, (iii) introduces HOCBF-mediated synergistic coupling between the soft robot and its environment demonstrated on the example of object manipulation, and (iv) presents DCSAT, a new, fast, and conservative differentiable collision-detection method for arbitrary convex geometries, improving the feasibility of real-time use for full-body safety guarantees.

II. BACKGROUND

This section introduces the main concepts for soft robot modeling, along with the definitions of HOCBFs and HOCLFs. For clarity and simplicity, we focus on the planar case throughout this letter, though the framework naturally generalizes to three-dimensional scenarios.

A. Soft Robotic Kinematics and Dynamics

We model the soft robot kinematics using the PCS formulation [19], which approximates the continuous backbone by discretizing it into N segments. Each segment i is characterized by a spatially constant strain vector $\xi_i = [\kappa_{be,i} \ \sigma_{sh,i} \ \sigma_{ax,i}]^T \in \mathbb{R}^3$, where $\kappa_{be,i}$, $\sigma_{sh,i}$, and $\sigma_{ax,i}$ denote the bending, shear, and axial strains, respectively [20]. The robot configuration \mathbf{q} is then defined as the deviation of these strains from their equilibrium values, yielding a generalized coordinate vector $\mathbf{q} \in \mathbb{R}^{3N}$. Based on this kinematic model, the forward kinematics map $\chi = \pi(\mathbf{q}, s) : (0, L] \times \mathbb{R}^{3N} \rightarrow SE(2)$ returns the Cartesian position $\chi = [p_x \ p_y]^T$ at a given arc-length position s along the backbone, where p_x, p_y are the x- and y-positions, $L \in \mathbb{R}$ is the total arc length of the robot's centerline, the group $SE(2)$ denotes the special euclidean group in two dimensions. Differentiating this map with respect to the configuration results in the Jacobian $\mathbf{J}(\mathbf{q}, s) = \frac{\partial \pi(\mathbf{q}, s)}{\partial \mathbf{q}} \in \mathbb{R}^{2 \times 3N}$.

The corresponding dynamics can be derived leveraging established multibody modeling procedures [22], resulting in the following equations of motion:

$$\underbrace{\mathbf{M}(\mathbf{q}) \ddot{\mathbf{q}} + \mathbf{C}(\mathbf{q}, \dot{\mathbf{q}}) \dot{\mathbf{q}} + \mathbf{G}(\mathbf{q})}_{\text{Multibody dynamics}} + \underbrace{\mathbf{K} \mathbf{q} + \mathbf{D} \dot{\mathbf{q}}}_{\text{Elastic and dissipative forces}} = \underbrace{\mathbf{A}(\mathbf{q}) \mathbf{u}}_{\text{Actuation model}}, \quad (1)$$

where $\mathbf{M}(\mathbf{q}), \mathbf{C}(\mathbf{q}, \dot{\mathbf{q}}) \in \mathbb{R}^{3N \times 3N}$ are the mass and Coriolis matrices, respectively, $\mathbf{G}(\mathbf{q})$ captures gravitational effects, and $\mathbf{K}, \mathbf{D} \in \mathbb{R}^{3N \times 3N}$ are the linear stiffness and damping matrices, respectively. The actuation matrix $\mathbf{A}(\mathbf{q}) \in \mathbb{R}^{3N \times m}$ maps the actuation $\mathbf{u} \in \mathbb{R}^m$ into generalized torques.

B. High Order Control Barrier Functions and High Order Control Lyapunov Functions

The soft robot dynamics can be expressed in control-affine form as an ODE:

$$\dot{\mathbf{x}} = \underbrace{\begin{bmatrix} \dot{\mathbf{q}} \\ -\mathbf{M}^{-1}(\mathbf{C} \dot{\mathbf{q}} + \mathbf{G} + \mathbf{K} \mathbf{q} + \mathbf{D} \dot{\mathbf{q}}) \end{bmatrix}}_{f(\mathbf{x})} + \underbrace{\begin{bmatrix} \mathbf{0}_{3N \times m} \\ \mathbf{M}^{-1} \mathbf{A}(\mathbf{q}) \end{bmatrix}}_{g(\mathbf{x})} \mathbf{u}, \quad (2)$$

where $\mathbf{x} = [\mathbf{q}^T \ \dot{\mathbf{q}}^T]^T \in \mathbb{R}^n$ with $n = 6N$ is the soft robot state with the corresponding time derivative $\dot{\mathbf{x}} \in \mathbb{R}^n$, control input $\mathbf{u} \in \mathcal{U} \subset \mathbb{R}^m$, and locally Lipschitz continuous dynamics functions $f(\mathbf{x}) : \mathbb{R}^n \rightarrow \mathbb{R}^n$ and $g : \mathbb{R}^n \rightarrow \mathbb{R}^{n \times m}$.

For the definition of class \mathcal{K} function and forward-invariant set, relative degree, please refer to [18].

In many soft robotic control tasks, constraints specified in task space do not yield an explicit dependence on the input \mathbf{u} after a single time derivative. This motivates the use of high-order extensions of CLFs and CBFs, where constraints are enforced on higher-order derivatives that expose the control input explicitly [18].

Given a function b with relative degree r , one can recursively construct a HOCBF or HOCLF as follows.

Definition 1 (High-Order Control Barrier Function [18]): Let $b : \mathbb{R}^n \rightarrow \mathbb{R}$ be a differentiable function with relative degree r with respect to the system (2). Define a sequence of functions recursively as:

$$\psi_0(\mathbf{x}) := b(\mathbf{x}),$$

$$\psi_i(\mathbf{x}) := L_f \psi_{i-1}(\mathbf{x}) + \alpha_i(\psi_{i-1}(\mathbf{x})), \quad i = 1, \dots, r-1,$$

where each α_i is a class- \mathcal{K} function. For each ψ_i , we define a corresponding safe set:

$$C_i := \{ \mathbf{x} \in \mathbb{R}^n : \psi_{i-1}(\mathbf{x}) \geq 0 \}, \quad i \in \{1, \dots, r\}.$$

Then, b is a *HOCBF* if there exists a final class- \mathcal{K} function α_r such that

$$\sup_{\mathbf{u} \in \mathcal{U}} [L_f^r b(\mathbf{x}) + L_g L_f^{r-1} b(\mathbf{x}) \mathbf{u} + O(b(\mathbf{x})) + \alpha_r(\psi_{r-1}(\mathbf{x}))] \geq 0, \quad \forall \mathbf{x} \in \cap_{i=1}^r C_i,$$

where L_f, L_g denote the Lie derivatives along f and g respectively, $O(\cdot)$ denotes the remaining Lie derivatives along f and partial derivatives with respect to t with degree less than or equal to $r-1$.

HOCBFs generalize CBFs [6] (i.e., a HOCBF with $r = 1$ is a CBF) [23].

Definition 2 (High-Order Control Lyapunov Function [23]): For a r th-order differentiable Lyapunov function $V : \mathbb{R}^n \times [t_0, \infty) \rightarrow \mathbb{R}$, we define the sequence of functions recursively $\phi_0(\mathbf{x}) := V(\mathbf{x})$,

$$\phi_i(\mathbf{x}) := L_f \phi_{i-1}(\mathbf{x}) + \beta_i(\phi_{i-1}(\mathbf{x})), \quad i = 1, \dots, r-1,$$

with each β_i a class- \mathcal{K} function. Then V is called a *HOCLF* if there exists a final class- \mathcal{K}_∞ function β_r such that

$$\inf_{\mathbf{u} \in \mathcal{U}} [L_f^r V(\mathbf{x}) + L_g L_f^{r-1} V(\mathbf{x}) \mathbf{u} + O(V(\mathbf{x})) + \beta_r(\phi_{r-1}(\mathbf{x}))] \leq 0, \quad \forall \mathbf{x} \neq \mathbf{0}_n.$$

The HOCBF (1), and the HOCLF (2) can be integrated into a Quadratic Program (QP) convex optimization problem:

$$\begin{aligned} \min_{\mathbf{u}, \delta} \quad & \|\mathbf{u}\|_2^2 + p \delta^2, \\ \text{s.t.} \quad & L_f^r b(\mathbf{x}) + L_g L_f^{r-1} b(\mathbf{x}) \mathbf{u} + O(b(\mathbf{x})) + \alpha_r(\psi_{r-1}(\mathbf{x})) \geq 0, \\ & L_f^r V(\mathbf{x}) + L_g L_f^{r-1} V(\mathbf{x}) \mathbf{u} + O(V(\mathbf{x})) + \beta_r(\phi_{r-1}(\mathbf{x})) \leq \delta. \end{aligned} \quad (3)$$

To keep the QP feasible when several HOCBFs and HOCLFs

contradict each other, we add a non-negative slack $\delta \geq 0$ with penalty $p > 0$. This slack relaxes safety constraints when strict enforcement is impossible due to the nominal input or mutual conflicts. Typically, HOCLFs capture performance objectives and HOCBFs safety and other constraints; assigning slack to lower-priority terms lets the controller trade performance for safety.

III. HIGH-ORDER CONTROL BARRIER AND LYAPUNOV FUNCTION FOR ENVIRONMENT-AWARE CONTROL

This section describes how we can design HOCBFs and HOCLFs for environment-aware soft robot control. Although our method is also applicable to 3D motions, we specialize the notation in this letter to the 2D case. Most importantly, we can ensure contact force limits, and with this safety, by deploying HOCBFs while relying on HOCLFs for defining motion behavior and objectives. To enable this, we require access to differentiable algorithms that perform collision detection and resolution between the soft robot body and convex polygonal environment obstacles. Subsequently, we elevate this framework to a more general coupling between the soft robot and its environment. Specifically, we consider a manipulation scenario and we demonstrate how our approach allows the soft robot to manipulate objects where contact is ensured via HOCBFs and the manipulation objectives are defined via HOCLFs.

We consider a planar soft robotic arm operating within a two-dimensional workspace $\mathcal{W} \subset \mathbb{R}^2$, populated by n_{obs} known convex obstacles $\mathcal{W}_{\text{obs}} = \{\mathcal{O}_1, \dots, \mathcal{O}_{n_{\text{obs}}}\}$. We also assume the robot is fully actuated, with $m = 3N = \frac{n}{2}$.

A. Collision Detection

To facilitate collision detection and spatial reasoning, the soft robotic arm, though continuously deformable, is approximated as a discrete chain of convex polygonal parts, as illustrated in Fig. 2. Specifically, the robot is segmented into N_{srpoly} convex polygons $\mathcal{R} = (P_1, \dots, P_{N_{\text{srpoly}}})$, each defined by its vertices $\{\mathbf{v}_{i,1}, \dots, \mathbf{v}_{i,k_i}\}$, where k_i is the number of vertices of the i th part. These vertices are computed via the forward kinematics $\pi(\mathbf{q}, s)$ defined earlier. Each polygon is represented as:

$$P_i = \left\{ \mathbf{x} \in \mathbb{R}^2 \mid \mathbf{x} = \sum_{j=1}^{k_i} \alpha_{i,j} \mathbf{v}_{i,j}, \alpha_{i,j} \geq 0, \sum_{j=1}^{k_i} \alpha_{i,j} = 1 \right\}. \quad (4)$$

The entire robot is then $\mathcal{R} = (P_i)_{i=1}^{N_{\text{srpoly}}}$.

This definition now allows us to detect collisions between the N_{srpoly} polygons approximating the robot body and the environment approximated by N_{obs} convex polygons. In order to do so, we need to know the configuration-dependent distance $h_{i,j}(\mathbf{q}) : \mathbb{R}^{3N} \rightarrow \mathbb{R}$ between the i th soft robot's part P_i and the j th obstacle \mathcal{O}_j . Here, a positive $h_{i,j}(\mathbf{q})$ indicates separation, while a negative value indicates penetration. This distance is provided by a polygon distance metric $d(\cdot, \cdot)$ s.t. $h_{i,j}(\mathbf{q}) = d(P_i(\mathbf{q}), \mathcal{O}_j)$, $i = 1, \dots, N_{\text{srpoly}}$, $j = 1, \dots, n_{\text{obs}}$, between the i th soft robot's part P_i and the j th obstacle \mathcal{O}_j . For notational simplicity, we omit the explicit dependence on the configuration variable \mathbf{q} and write $h_{i,j}$ in the remainder of this section. In principle, any differentiable distance function $d(\cdot, \cdot)$ can be used. In Section IV-B, we present DCSAT, which is a differentiable, computationally efficient, and conservative version of the SAT algorithm.

B. Collision Resolution

The distance metric $h_{i,j}(\mathbf{q})$ now allows us to resolve the collision, which means that we project the collision forces onto the soft robot dynamics and vice versa. In this work, we

specifically, without loss of generality, use a linear spring-damper model to capture the collision characteristics. Future work might explore more advanced contact models here. The collision force $F \in \mathbb{R}$ is given as

$$F(h_{i,j}, \dot{h}_{i,j}) = \begin{cases} 0, & \text{if } h_{i,j} > 0 \\ -k h_{i,j} - c \dot{h}_{i,j}, & \text{if } h_{i,j} \leq 0 \end{cases}$$

where k the contact stiffness, and c the damping coefficient. To recover differentiability, we approximate the collision dynamics as

$$F(h_{i,j}, \dot{h}_{i,j}) = k \log \left(1 + e^{-h_{i,j}/\varepsilon} \right) + c \log \left(1 + e^{-\dot{h}_{i,j}/\varepsilon} \right). \quad (5)$$

This contact force can now easily be applied to both the environment and the soft robot by projecting it along the contact surface vector. Specifically, for a given surface normal $\mathbf{n} \in \mathbb{R}^2$ with $\|\mathbf{n}\|_2 = 1$, the generalized contact torque onto the soft robot is given as $-\mathbf{J}^\top(\mathbf{q}) F \mathbf{n}$.

C. Ensuring Safety via High-Order Control Barrier Functions

Below, we introduce a set of relative-degree-two HOCBFs dedicated to maintaining safety. We start with an HOCBFs that is standard in rigid-robotics applications and ensures complete avoidance of contact between the robot and its environment. While effective, these constraints can sharply curb performance, encourage overly cautious behavior, and block truly collaborative human-robot interactions.

To overcome such drawbacks, we highlight a HOCBF limiting the contact force to $F_{\text{max}} \in \mathbb{R}_{>0}$. This approach allows controlled contact between the soft robot and its surroundings while guaranteeing that such contact remains safe [10]. Our formulation is inspired by extensive studies on injury-severity criteria for rigid collaborative robots [3] and by ISO/TS 15066:2016 [15], which specifies body-part-dependent force thresholds as proxies for injury risk.

- 1) **Contact Avoidance HOCBF:** To ensure safety with respect to a forbidden region $\mathcal{A} \subset \mathcal{W}$, we define a HOCBF based on the signed distance between the robot segment P_i and \mathcal{A} . Let $r \geq 0$ be a prescribed safety margin. Using the previously defined smooth distance metric $h_{i,\mathcal{A}}(\mathbf{q}) = d(P_i(\mathbf{q}), \mathcal{A})$, we define

$$b_{i,\mathcal{A}}(\mathbf{x}) = h_{i,\mathcal{A}}(\mathbf{q})^2 - r^2.$$

Then $b_{i,\mathcal{A}}(\mathbf{x}) \geq 0$ guarantees that P_i maintains a distance of at least $r \geq 0$ from \mathcal{A} .

- 2) **Contact Force Limit HOCBF:** For each obstacle $\mathcal{O}_j \in \mathcal{W}_{\text{obs}}$, define

$$b_{i,j}(\mathbf{x}) = F_{\text{max},j} - F(h_{i,j}, \dot{h}_{i,j}),$$

where $F(h_{i,j}, \dot{h}_{i,j})$ is the contact force, for example, stemming from a linear spring-damper contact model as defined in (5), and $F_{\text{max},j}$ is maximum allowable contact force in static settings as, for example, defined in ISO/TS 15066:2016 [15]. This barrier function ensures that the contact force between the i th soft robot part and the j th obstacle remains below the threshold.

D. Achieving Effective Motion Behavior via Higher-Order Control Lyapunov Functions

With the barrier conditions established, the next step is to deploy controllers that can generate effective motion. One option is a nominal controller—either model-based (e.g., PD+ feedforward [22]) or model-free (e.g., reinforcement learning [24])—subsequently filtered to guarantee safety [10]. In this letter, however, we focus on HOCLFs, which lets us articulate motion objectives highly intuitively

and flexibly. Any of the HOCLFs discussed below can, moreover, be “mixed and matched” with the HOCBFs described in the previous subsection.

- 1) **Error-Based Configuration Space Regulation HOCLF:** Let $\mathbf{q}, \mathbf{q}^d \in \mathbb{R}^{3N}$ be the actual and desired configuration of the soft robot, respectively. Then the error-based HOCLF function

$$V_{\text{csr},i}(\mathbf{x}) = \|\mathbf{q} - \mathbf{q}^d\|_2^2$$

encourages convergence of the soft robot towards the target shape.

- 2) **Task Space Regulation HOCLF:** Let $\mathbf{p}_i(\mathbf{q}) \in \mathbb{R}^2$ be the Cartesian pose of the tip of the i th segment and $\mathbf{p}_{\text{goal}} \in \mathbb{R}^2$ the desired target. Then the HOCLF function

$$V_{\text{tsr},i}(\mathbf{x}) = \|\mathbf{p}_i(\mathbf{q}) - \mathbf{p}_{\text{goal}}\|_2^2 \quad (6)$$

encourages convergence of the tip of the i th segment toward the target position.

- 3) **Contact Force Regulation HOCLF:** Contact force regulation, also frequently referred to as direct force control, is an important objective in (soft) robotics [25] that can also be achieved via HOCLFs. Specifically, to regulate the magnitude of the contact force toward a desired value $F^d \in \mathbb{R}$, we define

$$V_{\text{f},i,j}(\mathbf{x}) = \left(F(h_{i,j}, \dot{h}_{i,j}) - F^d\right)^2, \quad (7)$$

where $F(h_{i,j}, \dot{h}_{i,j})$ is the smooth linear spring-damper contact force defined earlier. Minimizing $V_{\text{f},i,j}$ drives the actual contact force toward F^d .

E. Achieving Synergistic Interaction Between Soft Robot and Environment: An Example of Object Manipulation

So far, we have focused on enforcing safety constraints between the soft robot and its environment via barrier functions. However, we can also establish a more general, synergistic coupling between the soft robot and its environment. As an example, we consider the scenario of object manipulation where the soft robot interacts with and moves a passive object through contact forces.

Let the system state be augmented as:

$$\mathbf{x} = [\mathbf{q}^\top \quad \dot{\mathbf{q}}^\top \quad \mathbf{x}_{\text{obj}}^\top \quad \dot{\mathbf{x}}_{\text{obj}}^\top]^\top \in \mathbb{R}^{6N+4},$$

where $\mathbf{x}_{\text{obj}} \in \mathbb{R}^2$ denotes the object's position in Cartesian space. The control objective is to steer \mathbf{x}_{obj} toward a target configuration $\mathbf{x}_{\text{obj,goal}}$. Under a contact force $\mathbf{F} \in \mathbb{R}^2$ applied at the robot tip via the positional Jacobian $\mathbf{J}(\mathbf{q}, s) \in \mathbb{R}^{2 \times 3N}$, the system evolves under the control-affine dynamics:

$$\dot{\mathbf{x}} = \underbrace{\begin{bmatrix} \dot{\mathbf{q}} \\ \dot{\mathbf{x}}_{\text{obj}} \\ -M^{-1}(C\dot{\mathbf{q}} + \mathbf{G} + \mathbf{K}\mathbf{q} + D\dot{\mathbf{q}} + \mathbf{J}^T\mathbf{F}) \\ -m_o^{-1}\mathbf{F} \end{bmatrix}}_{f(\mathbf{x})} + \underbrace{\begin{bmatrix} \mathbf{0}_{3N \times m} \\ \mathbf{0}_{2 \times m} \\ M^{-1}\mathbf{A} \\ \mathbf{0}_{2 \times m} \end{bmatrix}}_{g(\mathbf{x})} \mathbf{u}, \quad (8)$$

where m_o is the mass of the to-be-manipulated object.

a) **Task Decomposition:** Observe that in (8), the control input \mathbf{u} does not directly affect \mathbf{x}_{obj} . Therefore, effective object manipulation must rely on indirect influence via contact forces between the robot and the object. We thus decompose the task into two stages:

- 1) **Contact Containment via HOCBF:** Drive the robot's end-effector to a designated contact location \mathbf{x}_{cont} on the object surface to enable effective pushing.
- 2) **Object Regulation via HOCLF:** Apply the contact force to steer the object from its current state \mathbf{x}_{obj} to the goal state $\mathbf{x}_{\text{obj}}^d$.

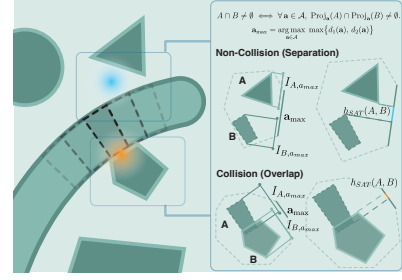


Fig. 2: **Illustration of SAT Polygon Distance Metrics.** Visualization of SAT-based polygon distance metrics used for collision detection between the soft robot body and convex polygonal obstacles. Specifically, we illustrate the definition of the signed distance $h_{\text{SAT}}(A, B)$ between convex polygons A and B . The right panel shows projection intervals $I_{A,a}$ and $I_{B,a}$ along the maximizing axis a_{max} in both separation (top) and overlap (bottom) scenarios.

b) **Contact Containment HOCBF:** We define the barrier function to ensure contact between the soft robot and the object

$$b_{\text{ca}}(\mathbf{x}) = \epsilon - \|\mathbf{x}_{\text{ee}}(\mathbf{x}) - \mathbf{x}_{\text{cont}}\|_2^2,$$

where $\epsilon > 0$, $\mathbf{x}_{\text{ee}}(\mathbf{q}) \in \mathbb{R}^2$ is the Cartesian position of the end-effector and $\mathbf{x}_{\text{cont}} \in \mathbb{R}^2$ is a predefined contact target on the object. This function has relative degree two, and a recursive HOCBF can be constructed to enforce convergence to the contact surface while respecting system dynamics.

c) **Object Regulation HOCLF:** To guide the object to its goal, we define the Lyapunov function

$$V_{\text{or}}(\mathbf{x}) = \|\mathbf{x}_{\text{obj}}(\mathbf{x}) - \mathbf{x}_{\text{obj}}^d\|_2^2,$$

which has a relative degree of three due to the indirect actuation via contact. A recursive HOCLF can then be derived to ensure asymptotic convergence to the object goal configuration while remaining compatible with the contact dynamics.

IV. DIFFERENTIABLE POLYGON DISTANCE METRIC

For HOCBF constructions requiring an r th-order continuously differentiable distance metric, the classical SAT [26], despite its efficiency for convex polygons and widespread use over support mapping methods such as the Gilbert-Johnson-Keerthi (GJK) algorithm [27], is fundamentally unsuitable due to its reliance on non-smooth min and max operations. This lack of differentiability prevents its direct application in force- or distance-based high-order control formulations. To address this limitation, prior work has introduced a differentiable variant of SAT, named SSAT, that approximates these non-differentiable operations using multi-level smoothing techniques to achieve C^∞ continuity [21]. However, the SSAT overestimates the polygon separation distance, which can lead to a violation of the safety constraint in downstream applications. In this letter, we propose a new differentiable variant of SAT, coined DCSAT, which replaces the layered smoothing pipeline of SSAT [21] with a single LogSumExp (LSE) approximation while providing a conservation metric for calculating distance between convex polygons. DCSAT preserves the C^∞ differentiability required for high-order control while significantly simplifying implementation and reducing computational overhead.

A. Baselines: SAT and SSAT

Before defining our distance metrics, we briefly revisit the SAT framework, which forms the foundation of convex polygon-distance computations based on orthogonal projections.

Definition 3 (Separating axis): Let $A, B \subset \mathbb{R}^d$ be convex sets. A unit vector $\mathbf{a} \in \mathbb{R}^d$ is called a *separating axis* for A and B if the projections of the sets onto \mathbf{a} are disjoint; that is, if either

$$\max_{x \in A} \mathbf{a}^\top x < \min_{y \in B} \mathbf{a}^\top y \quad \text{or} \quad \max_{y \in B} \mathbf{a}^\top y < \min_{x \in A} \mathbf{a}^\top x.$$

Theorem 1 (Separating Axis Theorem [26]): Two convex sets A and B in \mathbb{R}^d are disjoint if and only if there exists a separating axis between them.

Lemma 1 (Sufficiency of Edge Normals in \mathbb{R}^2): Let $A, B \subset \mathbb{R}^2$ be convex polygons. Then it suffices to test for separation along the set of directions orthogonal to the edges of A and B . Specifically, let $S(A)$ and $S(B)$ denote the sets of edge directions of A and B , respectively. Define

$$\mathcal{A} = \{\ell^\perp : \ell \in S(A) \cup S(B)\}, \quad (9)$$

where ℓ^\perp denotes the unit vector orthogonal to edge ℓ . Then \mathcal{A} is a complete set of candidate separating axes.

Proof. By the Separating Axis Theorem (Theorem 1), if A and B are disjoint, there exists a direction $\mathbf{n} \in \mathbb{S}^1$ such that their projections onto \mathbf{n} do not overlap:

$$\max_{x \in A} \mathbf{n}^\top x < \min_{y \in B} \mathbf{n}^\top y \quad \text{or} \quad \max_{y \in B} \mathbf{n}^\top y < \min_{x \in A} \mathbf{n}^\top x.$$

Since the support function of a convex polygon is piecewise linear and attains its extrema at vertices, any separating direction must be orthogonal to some edge of A or B . Therefore, it suffices to test separation along directions in \mathcal{A} . If no such direction yields separation, A and B must intersect. \square

By combining Theorem 1 and Lemma 1, separation testing—and more specifically, the computation of separating distances—can be reduced to a finite set of one-dimensional projections. These observations underlie the projection-based metrics (SAT, SSAT, DCSAT) used throughout this letter.

a) SAT distance metric: Following by the above statements, we could derive the distance between two polygons A and B .

Projections. Let $\mathbf{A}_i, i \in \mathcal{I}_A, \mathbf{B}_j, j \in \mathcal{I}_B$ denote the vertices of convex sets A, B , respectively, where \mathcal{I}_A and \mathcal{I}_B denote the index sets of the vertices of A, B respectively. For each axis $\mathbf{a} \in \mathcal{A}$, the scalar projections of polygon vertices \mathbf{A}_i for $i \in \mathcal{I}_A$, and \mathbf{B}_j for $j \in \mathcal{I}_B$, onto \mathbf{a} are defined as

$$A_{i,a} = \mathbf{a}^\top \mathbf{A}_i, \quad B_{j,a} = \mathbf{a}^\top \mathbf{B}_j.$$

Per-axis distance. The signed separation (positive if separated, negative if overlapping) between the projected intervals along axis \mathbf{a} is given by

$$\begin{aligned} d_1(\mathbf{a}) &= \min_{j \in \mathcal{I}_B} B_{j,a} - \max_{i \in \mathcal{I}_A} A_{i,a}, \\ d_2(\mathbf{a}) &= \min_{i \in \mathcal{I}_A} A_{i,a} - \max_{j \in \mathcal{I}_B} B_{j,a}, \end{aligned} \quad (10)$$

$$g_{\text{SAT}}(\mathbf{a}) = \max\{d_1(\mathbf{a}), d_2(\mathbf{a})\}.$$

Global metric. The overall SAT-based signed distance between polygons A and B is then defined as

$$h_{\text{SAT}}(A, B) = \max_{\mathbf{a} \in \mathcal{A}} g_{\text{SAT}}(\mathbf{a}). \quad (11)$$

This value is positive when the polygons are separated, zero if they touch, and negative when they overlap.

b) Smooth SAT (SSAT) distance metric: To enable differentiable collision-aware control, the SSAT method [21] provides a C^∞ approximation of the classical SAT by replacing non-smooth operations with differentiable surrogates.

Definition of geometric terms. Let $\Delta p_{A,B} \in \mathbb{R}^3$ be the vector from the center of cuboid A to the center of cuboid B , and $r_{jk} \in \mathbb{R}^2$ represent the half-dimensions of object

$j \in \{A, B\}$ along direction $k \in \{x, y\}$. The scalar projection of these vectors onto axis $\mathbf{a} \in \mathcal{A}$ forms the basis of the separation metric.

Smooth absolute-value surrogate. To replace the non-differentiable absolute value $|x|$, the method uses the smooth surrogate

$$f_{\text{sabs}}(x) = x \tanh(\alpha_{\text{sabs}} x),$$

where $\alpha_{\text{sabs}} > 0$ controls the sharpness. This function is C^∞ , odd-symmetric, and converges pointwise to $|x|$ as $\alpha_{\text{sabs}} \rightarrow \infty$.

Smooth separation per axis. For each axis \mathbf{a} , the signed distance is approximated as

$$g_{\text{SSAT}}(\mathbf{a}) = f_{\text{sabs}}(\mathbf{a}^\top \Delta p_{A,B}) - \sum_{j \in \{A, B\}} \sum_{k \in \{x, y, z\}} f_{\text{sabs}}(\mathbf{a}^\top r_{jk}),$$

where the first term captures the projected distance between cuboid centers, and the second term approximates the combined extent of both bodies along axis \mathbf{a} . When $g_{\text{SSAT}} > 0$, the bodies are separated along axis n_i .

Smooth global aggregation. The final SSAT metric is computed by replacing the outer maximum over axes with a soft maximum using the LogSumExp (LSE) function:

$$h_{\text{SSAT}}(A, B) = \frac{1}{\alpha_{\text{max}}} \log \sum_{\mathbf{a} \in \mathcal{A}} \exp(\alpha_{\text{max}} g_{\text{SSAT}}(\mathbf{a})),$$

where $\alpha_{\text{max}} > 0$ is a smoothing parameter. The resulting metric is C^∞ for all finite values of α_{sabs} and α_{max} , and recovers the exact SAT distance in the limit $\alpha_{\text{sabs}}, \alpha_{\text{max}} \rightarrow \infty$.

B. Differentiable Conservative SAT (DCSAT)

To enable safe and differentiable distance evaluation for use in HOCBF+HOCLF controllers, and resolve the underestimation of the polygon extents present in SSAT [21], we introduce the DCSAT metric, which provides a conservative estimate of the polygon separation/penetration distance at an increased computational efficiency compared to SSAT. Unlike SSAT, which smooths each intermediate geometric operation and is primarily designed for quadrilateral shapes, DCSAT operates directly on global signed separation distances. It applies a single LSE operation to obtain a C^∞ approximation of the SAT metric that naturally extends to arbitrary convex polygons. Furthermore, DCSAT consistently underestimates the true separation distance, ensuring that safety constraints enforced via control barrier functions remain valid even under model uncertainty or near-contact conditions. This makes it particularly suitable for collision-aware control of systems with complex geometries.

Definition 4 (Differentiable Conservative SAT (DCSAT)): Let $A, B \subset \mathbb{R}^2$ be convex polygons, and let \mathcal{A} denote the set of separating axes as defined in 9. For each axis $\mathbf{a} \in \mathcal{A}$, define the separation terms $d_1(\mathbf{a})$ and $d_2(\mathbf{a})$ as in (10). Let

$$\mathcal{D} = \{d_m(\mathbf{a}) \mid \mathbf{a} \in \mathcal{A}, m \in \{1, 2\}\}.$$

Then the DCSAT distance is defined as

$$h_{\text{DCSAT}}(A, B) := \frac{1}{\alpha_{\text{max}}} \log \left(\sum_{d \in \mathcal{D}} e^{\alpha_{\text{max}} d} \right) - \frac{\log(2|\mathcal{A}|)}{\alpha_{\text{max}}}.$$

Lemma 2 (Bounds for DCSAT):

$$-\frac{\log(2|\mathcal{A}|)}{\alpha_{\text{max}}} \leq h_{\text{DCSAT}}(A, B) - h_{\text{SAT}}(A, B) \leq 0.$$

Proof. Let $M = \max \mathcal{D} = h_{\text{SAT}}(A, B)$, and define

$$e := \frac{1}{\alpha_{\text{max}}} \log \left(\sum_{d \in \mathcal{D}} e^{\alpha_{\text{max}} d} \right).$$

Lower bound: One term in the sum is $e^{\alpha_{\text{max}} M}$, so

$$\begin{aligned} \sum e^{\alpha_{\max} d} &\geq e^{\alpha_{\max} M} \Rightarrow e \geq M \\ &\Rightarrow h_{\text{DCSAT}}(A, B) - M \geq -\frac{\log(2|\mathcal{A}|)}{\alpha_{\max}}. \end{aligned}$$

Upper bound: Since $|\mathcal{D}| = 2|\mathcal{A}|$, we have

$$\begin{aligned} \sum e^{\alpha_{\max} d} &\leq 2|\mathcal{A}| \cdot e^{\alpha_{\max} M} \Rightarrow e \leq M + \frac{\log(2|\mathcal{A}|)}{\alpha_{\max}} \\ &\Rightarrow h_{\text{DCSAT}}(A, B) - M \leq 0. \end{aligned}$$

□

Theorem 2 (Conservative Approximation via DCSAT): Let

$$e := \frac{1}{\alpha_{\max}} \log \left(\sum_{d \in \mathcal{D}} e^{\alpha_{\max} d} \right), h_{\text{DCSAT}}(A, B) := e - \frac{\log(2|\mathcal{A}|)}{\alpha_{\max}}.$$

Then:

- (a) $h_{\text{DCSAT}}(A, B) \in C^\infty$,
- (b) $h_{\text{DCSAT}}(A, B) \leq h_{\text{SAT}}(A, B)$ for all A, B ,
- (c) If $h_{\text{DCSAT}}(A, B) = 0$, then the true SAT distance satisfies

$$0 \leq h_{\text{SAT}}(A, B) < \frac{\log(2|\mathcal{A}|)}{\alpha_{\max}}.$$

Proof. (a) Since e is composed of exponential and logarithmic operations over a finite sum of smooth terms, it follows that $e \in C^\infty$. Subtracting a constant preserves smoothness, hence $h_{\text{DCSAT}} \in C^\infty$.

(b) Follows directly from Lemma 2.

(c) If $h_{\text{DCSAT}}(A, B) = 0$, then by definition,

$$e = \frac{\log(2|\mathcal{A}|)}{\alpha_{\max}}.$$

From Lemma 2, it follows that

$$h_{\text{SAT}}(A, B) \leq \frac{\log(2|\mathcal{A}|)}{\alpha_{\max}}.$$

Since $h_{\text{DCSAT}} \leq h_{\text{SAT}}$, with $h_{\text{DCSAT}} = 0$

$$0 \leq h_{\text{SAT}}(A, B) \leq \frac{\log(2|\mathcal{A}|)}{\alpha_{\max}}.$$

which confirms the conservative approximation of the real distance: if the smoothed metric DCSAT hits zero, the true SAT distance remains non-negative. □

The DCSAT procedure is summarized in Algorithm 1.

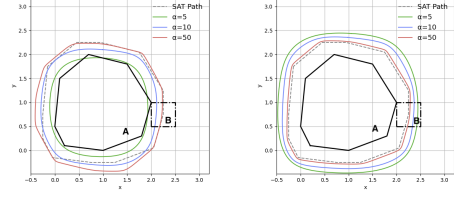
Algorithm 1 Differentiable Conservative SAT (DCSAT)

Require: Convex polygons $A = \{\mathbf{A}_i\}$, $B = \{\mathbf{B}_j\}$; sharpness $\alpha > 0$

- 1: $\mathcal{A} \leftarrow \{\ell^\perp : \ell \in S(A) \cup S(B)\}$
 - 2: **for all** $\mathbf{a} \in \mathcal{A}$ **do**
 - 3: $d_1 \leftarrow \min_j (\mathbf{a}^\top \mathbf{B}_j) - \max_i (\mathbf{a}^\top \mathbf{A}_i)$
 - 4: $d_2 \leftarrow \min_i (\mathbf{a}^\top \mathbf{A}_i) - \max_j (\mathbf{a}^\top \mathbf{B}_j)$
 - 5: Add d_1, d_2 to \mathcal{D}
 - 6: **end for**
 - 7: $h \leftarrow \frac{1}{\alpha} \log \sum_{d \in \mathcal{D}} e^{\alpha d} - \frac{\log(2|\mathcal{A}|)}{\alpha}$
 - 8: **return** h
-

C. Benchmarking DCSAT

While the original SSAT formulation [21] was designed specifically for rectangles or axis-aligned quadrilaterals, its underlying principle—approximating projection half-extents using smooth absolute value functions—can be generalized to arbitrary convex shapes. To enable a fair comparison



(a) SSAT [21] vs. SAT (b) DCSAT (ours) vs. SAT

Fig. 3: Qualitative Benchmarking of DCSAT. Comparison of zero-level contours between smoothed / differentiable polygon distance metrics and the classical SAT. Specifically, we compare the position of the square polygon at a zero distance with the 8-sided polygon according to the respective distance metric. In both cases, we report the resulting contours for various sharpness parameters α , and the gray dashed curve represents the true zero-level set of the classical, but not differentiable SAT (i.e., the ground-truth), where the centroid of polygon B is in contact with polygon A . SSAT [21] exhibits underestimation of the polygon contour / an overestimation of the distance h_{SAT} , which can cause safety issues when used for formulating safety constraints. In contrast, the DCSAT (ours) contours consistently overestimate the contour boundary / underestimates the distance h_{SAT} , demonstrating a conservative and safety-preserving approximation.

TABLE I: Average runtime per distance evaluation (ms) on convex polygons of size N . The speedup is relative to the SSAT [21] implementation.

N	SAT (ms) ↓	SSAT (ms) ↓	DCSAT (ours) (ms) ↓	Speedup ↑
4	0.008	0.013	0.008	1.61
8	0.007	0.035	0.023	1.52
16	0.023	0.042	0.025	1.65
32	0.021	0.055	0.020	2.73

across general geometries, we implemented this natural extension and evaluated it against our proposed DCSAT and the classical SAT [26].

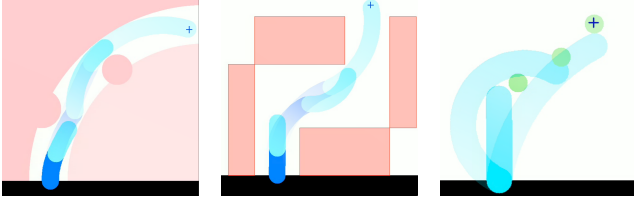
Fig. 3 visualizes the zero-level contours of both smooth metrics relative to the classical SAT boundary. Notably, DCSAT consistently generates a conservative underestimation of the true separation distance, ensuring that the smoothed constraint remains valid under model error or near-contact conditions. In contrast, SSAT [21] tends to overestimate the true separation at low sharpness levels, which can compromise safety-critical guarantees in barrier-based control.

Although both smoothed variants are implemented efficiently in JAX, DCSAT achieves comparable or better computational performance compared to SSAT [21] despite its global formulation. As shown in Table I, it maintains fast execution across polygon sizes while preserving full C^∞ smoothness. Taken together, these results suggest that DCSAT offers a robust and practical surrogate to classical SAT for use in applications that require differentiability and a conservative approximation of the polygon separation distance.

V. EXPERIMENTS

We demonstrate the effectiveness and possibility of our proposed methodology, as shown in Fig. 4. We first evaluate the effectiveness of the proposed HOCBF+HOCLF controller on two navigation scenarios in simulation. Secondly, we present a novel application of HOCBF+HOCLF by considering an object manipulation task.

We build on the CBFpy [28] package that offers an easy-to-use and high-performance implementation of (high-order) CBF+CLF in JAX while leveraging analytical gradients obtained via autodifferentiation. In all simulations, we assume without loss of generality an identity actuation matrix



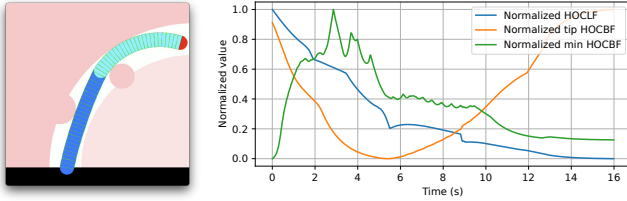
(a) **Medical Scenario** (e.g., endoscopy): a continuum soft robot navigates a curved pass-environment while ensuring contact force limits to its to prevent damage to ensure safety. (b) **Search & Rescue**: the robot threads through a cluttered rectangular environment while ensuring contact force limits to the soft robot. (c) **Object Manipulation**: the robot tip pushes a green sphere toward the target (blue cross) while ensuring the robot and the object stay in contact.

Fig. 4: Application Cases. Applications of the proposed HOCBF-HOCLF control framework in three representative tasks. The blue-to-white gradient shows the evolution of the soft robot’s shape over time. The blue cross marks the objectives.

$\mathbf{A}(\mathbf{q}) = \mathbb{I}_{3N}$. When plotting the results, all time-series data $x(t)$ (e.g., contact force F , HOCBF, HOCLF, and control input norms $\|\mathbf{u}(t)\|_2$) is normalized to the range $[0, 1]$ using standard min-max scaling:

$$x_{\text{norm}}(t) = \frac{x(t) - x_{\min}}{x_{\max} - x_{\min} + \varepsilon},$$

where $\varepsilon = 10^{-8}$ prevents division by zero. For fair comparison across control strategies, a global normalization is applied when comparing the same quantity across different policies.



(a) Collision detection by approximating robot as a chain of polygons (b) Normalized HOCBF/HOCLF evolution

Fig. 5: Results for Medical Scenario. The task is specified using a *task space regulation HOCLF* and safety is ensured via *contact force limit HOCBFs*. **Panel (a):** The soft robot is segmented into convex polygonal parts (thin green lines) for spatially distributed collision detection, resolution, and enforcement of safety barriers. **Panel (b):** Normalized evolution of the HOCLF value, the HOCBF value at the robot tip/end-effector, and the minimum HOCBF value across the soft robot.

A. Navigation Simulations

We first demonstrate the application of the proposed control framework in contact safety-aware navigation scenarios - specifically medical and search & rescue tasks, as shown in Fig. 4(a) and Fig. 4(b), respectively. For both tasks, we employ *Contact Force Limit HOCBFs* (along the entire soft robot body) for ensuring safety and a *Task Space Regulation HOCLF* to specify the end-effector navigation goal.

In Fig. 5(b), we consider the *medical scenario* and show the normalized evolution of the HOCLF, the HOCBF at the tip, and the minimum HOCBF value over time. The HOCLF value steadily converges toward zero, indicating task completion, while both HOCBF values remain positive, thereby ensuring persistent safety during motion.

Next, we conduct comparative experiments on the *search & rescue* scenario to underline the role of contact-force modulation. Three control schemes are assessed: (1) a safety-unaware controller—still common practice in

soft-robotics research [17]—that neglects safety constraints during optimization; (2) a contact-avoidance controller, typical in rigid-robotics contexts such as collision avoidance [2], [3]; and (3) our proposed contact-force-limit controller, which allows contact while bounding the maximum force. For numerical stability, strategy (1) is emulated by markedly loosening the contact-force limits in the HOCBF, whereas strategy (2) is obtained by setting those limits virtually to zero. We show the results in Fig. 6 and Fig. 7 as sequences of stills and time evolution plots, respectively. Indeed, the results demonstrate that the *safety-unaware* controller (1) generates high contact forces that are potentially unsafe, (2) the *contact-avoidance* is not able to complete the task as it exhibits an overly conservative behavior and the soft robot is not able to exploit its embodied intelligence, and (3) the proposed *contact-force limit* exhibits very good task performance while preserving safety by restricting the maximum contact force.

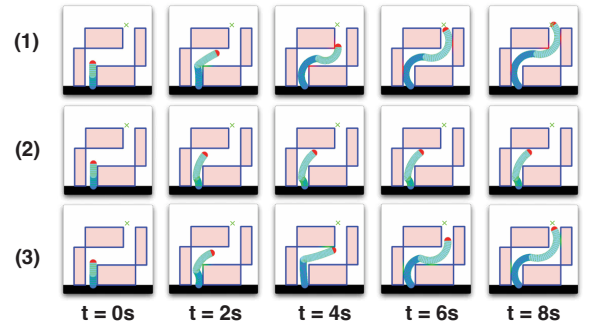


Fig. 6: Search & Rescue Sequence of Stills. Sequence of stills for the system evolution in the *search & rescue* scenario for three different control paradigms: (1) *safety-unaware control* (i.e., optimizing for the task objective instead of the safety constraints) as it is common in the state-of-the-art for soft robotic control [22], (2) *contact-avoidance control* which is the common paradigm in rigid robotics, and (3) *contact-force limit control* (ours) which embraces contact with the environment while ensuring safety via contact force limits. Contact interaction states are visualized with color cues: blue indicates no contact, green denotes safe contact, and red highlights contact above the maximum allowable force. The green cross denotes the task-space goal for this task.

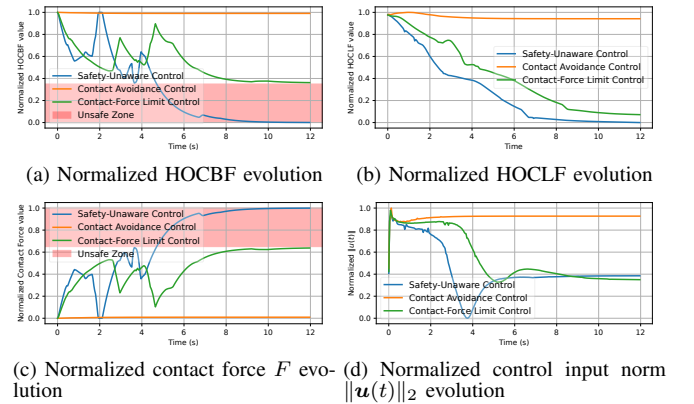
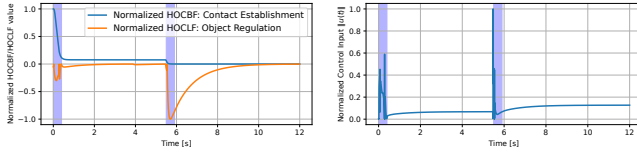


Fig. 7: Search & Rescue Time Evolution. Normalized time evolution of the HOCLF, the minimum HOCBF value, the minimum contact force, and the normalized control input norm across the robot for different controllers during a *search & rescue* scenario. Please refer to the caption of Fig. 6 for more details about the experiment and the considered controllers.

B. Object Manipulation Simulations

Finally, we demonstrate the application of the HOCBF+HOCLF control framework for object interaction,



(a) Normalized HOCBF and HOCLF evolution

(b) Normalized control input norm

Fig. 8: **Object Manipulation Metrics.** Time evolution of the normalized HOCBF, HOCLF, and control input norm $\|u(t)\|$ during the *object manipulation* scenario. Blue region indicates contact phases. For visualization of the physical behavior, refer to Fig. 4c.

as proposed in Section III-E, and depicted in Fig. 4(c). We evaluate the performance in a planar manipulation task involving repeated contact with a movable object. As shown in Fig. 8, the normalized HOCBF and HOCLF trajectories reveal distinct phases of interaction. Each drop in the HOCBF curve toward zero corresponds to the moment when the tip/effector of the soft robot establishes contact with the object, triggering the activation of the contact safety constraint. Notably, two such interactions occur, each pushing the object incrementally toward its goal.

During the initial contact phases, the HOCBF constraint is temporarily violated—an expected behavior due to the dynamics of rapid engagement. However, as the experiment evolves, the *Contact Containment* constraint value is gradually driven back toward zero, indicating that safe interaction is restored and maintained. Following the second contact, the HOCLF value decreases and steadily converges to zero, confirming that the object reaches its target and the overall system stabilizes. This experiment confirms the effectiveness of the proposed framework: the HOCBF successfully regulates contact between the soft robot and the object, while the HOCLF ensures that the object is persistently driven towards the desired position.

VI. CONCLUSION

This letter introduces a HOCBFs+HOCLFs framework [23] for the control of soft robots, grounded in a differentiable PCS model [19], [20] and a novel differentiable and conservative polygon distance metric DCSAT. Our method allows (1) soft robots to embrace contact with the environment but ensure safety via contact force-limit HOCBFs evaluated along the entire soft robot body, (2) the flexible and expressive specification of control objectives, such as shape and end-effector regulation or object manipulation, via HOCLFs. The DCSAT metric offers a C^∞ approximation of the classical SAT, yielding conservative signed distances with reduced computational overhead compared to existing baseline methods that overestimate the distance, leading to potentially unsafe behavior. Simulated experiments in navigation and object manipulation scenarios validate the framework’s ability to maintain geometric safety and guide soft robots toward task objectives. Building on these results, ongoing work is extending the framework to 3D simulations and experiments with multi-DOF soft robotic manipulators, where spatial reasoning, whole-body contact, and dynamic interactions become increasingly complex.

REFERENCES

[1] A. K. Hall, U. Backonja *et al.*, “Acceptance and perceived usefulness of robots to assist with activities of daily living and healthcare tasks,” *Assistive Technology*, 2019.

[2] S. Haddadin, A. Albu-Schaffer *et al.*, “Collision detection and reaction: A contribution to safe physical human-robot interaction,” in *2008 IEEE/RSJ International Conference on Intelligent Robots and Systems*. IEEE, 2008, pp. 3356–3363.

[3] S. Haddadin, *Towards safe robots: approaching Asimov’s 1st law*. Heidelberg: Springer Berlin, 2013, vol. 90.

[4] O. Khatib, “A unified approach for motion and force control of robot manipulators: The operational space formulation,” *IEEE Journal on Robotics and Automation*, vol. 3, no. 1, pp. 43–53, 1987.

[5] A. Pupa and C. Secchi, “Efficient iso/ts 15066 compliance through model predictive control,” in *2024 IEEE International Conference on Robotics and Automation (ICRA)*. IEEE, 2024, pp. 17 358–17 364.

[6] A. D. Ames, X. Xu *et al.*, “Control barrier function based quadratic programs for safety critical systems,” *IEEE Transactions on Automatic Control*, vol. 62, no. 8, pp. 3861–3876, 2016.

[7] F. Ferraguti, M. Bertuletti *et al.*, “A control barrier function approach for maximizing performance while fulfilling to iso/ts 15066 regulations,” *IEEE Robotics and Automation Letters*, vol. 5, no. 4, pp. 5921–5928, 2020.

[8] D. Rus and M. T. Tolley, “Design, fabrication and control of soft robots,” *Nature*, vol. 521, no. 7553, pp. 467–475, 2015.

[9] M. Stölzle, N. Pagliarini *et al.*, “Soft yet effective robots via holistic co-design,” *ArXiv.org*, 04 2025.

[10] A. K. Dickson, J. C. P. Garcia *et al.*, “Safe autonomous environmental control for soft robots using control barrier functions,” *arXiv preprint arXiv:2504.14755*, 2025.

[11] Q. Guan, F. Stella *et al.*, “Trimmed helicoids: an architected soft structure yielding soft robots with high precision, large workspace, and compliant interactions,” *npj Robotics*, vol. 1, no. 1, p. 4, 2023.

[12] D. A. Haggerty, M. J. Banks *et al.*, “Control of soft robots with inertial dynamics,” *Science robotics*, vol. 8, no. 81, p. eadd6864, 2023.

[13] O. Yasa, Y. Tshimitsu *et al.*, “An overview of soft robotics,” *Annual Review of Control, Robotics, and Autonomous Systems*, vol. 6, no. 1, pp. 1–29, 2023.

[14] Z. J. Patterson, W. Xiao *et al.*, “Safe control for soft-rigid robots with self-contact using control barrier functions,” in *2024 IEEE 7th International Conference on Soft Robotics (RoboSoft)*. IEEE, 2024, pp. 151–156.

[15] I. Standard, “Iso/ts 15066: 2016: Robots and robotic devices—collaborative robots,” *International Organization for Standardization: Geneva, Switzerland*, 2016.

[16] G. Mengaldo, F. Renda *et al.*, “A concise guide to modelling the physics of embodied intelligence in soft robotics,” *Nature Reviews Physics*, vol. 4, no. 9, pp. 595–610, 2022.

[17] C. Della Santina, R. K. Katzschmann *et al.*, “Model-based dynamic feedback control of a planar soft robot: trajectory tracking and interaction with the environment,” *The International Journal of Robotics Research*, vol. 39, no. 4, pp. 490–513, 2020.

[18] W. Xiao and C. Belta, “High-order control barrier functions,” *IEEE Transactions on Automatic Control*, vol. 67, no. 7, pp. 3655–3662, 2021.

[19] F. Renda, F. Boyer *et al.*, “Discrete cosserat approach for multisection soft manipulator dynamics,” *IEEE Transactions on Robotics*, vol. 34, no. 6, pp. 1518–1533, 2018.

[20] M. Stölzle, D. Rus, and C. Della Santina, “An experimental study of model-based control for planar handed shearing auxetics robots,” in *Experimental Robotics*. Cham: Springer Nature Switzerland, 2024, pp. 153–167.

[21] N. Takasugi, M. Kinoshita *et al.*, “Real-time perceptive motion control using control barrier functions with analytical smoothing for six-wheeled-telescopic-legged robot tachyon 3,” in *2024 IEEE/RSJ International Conference on Intelligent Robots and Systems (IROS)*. IEEE, 2024, pp. 6802–6809.

[22] C. Della Santina, C. Duriez, and D. Rus, “Model-based control of soft robots: A survey of the state of the art and open challenges,” *IEEE Control Systems Magazine*, vol. 43, no. 3, pp. 30–65, 2023.

[23] W. Xiao, C. A. Belta, and C. G. Cassandras, “High order control lyapunov-barrier functions for temporal logic specifications,” in *2021 American Control Conference (ACC)*. IEEE, 2021, pp. 4886–4891.

[24] R. Jitsho, T. G. W. Lum *et al.*, “Reinforcement learning enables real-time planning and control of agile maneuvers for soft robot arms,” in *Conference on Robot Learning*. PMLR, 2023, pp. 1131–1153.

[25] C. Della Santina, R. K. Katzschmann *et al.*, “Dynamic control of soft robots interacting with the environment,” in *2018 IEEE International Conference on Soft Robotics (RoboSoft)*. IEEE, 2018, pp. 46–53.

[26] W. Bittle, “Sat (separating axis theorem),” <https://dyn4j.org/2010/01/sat/>, 2010, accessed: 2025-04-29.

[27] E. G. Gilbert, D. W. Johnson, and S. S. Keerthi, “A fast procedure for computing the distance between complex objects in three-dimensional space,” *IEEE Journal of Robotics and Automation*, vol. 4, no. 2, pp. 193–203, 1988.

[28] D. Morton and M. Pavone, “Safe, task-consistent manipulation with operational space control barrier functions,” *arXiv preprint arXiv:2503.06736*, 2025, submitted to IEEE/RSJ International Conference on Intelligent Robots and Systems (IROS), Hangzhou, 2025.